Available online at www.sciencedirect.com
ScienceDirect
Journal of the European Ceramic Society 31 (2011) 401–408
www.elsevier.com/locate/jeurceramsoc

Micro- and macro-indentation behaviour of $Ba_{0.5}Sr_{0.5}Co_{0.8}Fe_{0.2}O_{3-d}$ perovskite

A. Chanda [a], B.X. Huang [b], J. Malzbender [b,*], R.W. Steinbrech [b]

[a] *Jadavpur University, Mechanical Engineering Department, Kolkata 700032, India*
[b] *Forschungszentrum Jülich GmbH, IEK-2, 52428 Jülich, Germany*

Received 27 July 2010; received in revised form 6 October 2010; accepted 12 October 2010
Available online 5 November 2010

Abstract

$Ba_{0.5}Sr_{0.5}Co_{0.8}Fe_{0.2}O_{3-d}$ (BSCF) is a candidate material for the application as oxygen separation membrane. However, the requisite mechanical reliability needs to be warranted. Indentation tests on dense BSCF yielded data for hardness, stiffness and fracture toughness up to a temperature of 340 °C. Complementary to this, the fracture toughness was also evaluated up to 800 °C based on an indentation-strength method.

Up to 200 °C, the values of all characteristic mechanical parameters decreased. At high temperatures they increased. The morphology of the indentation cracks depended on the applied indentation load. This was taken into account while selecting suitable expressions for calculating indentation toughness. The temperature dependence of the normalised fracture toughness as determined by indentation technique and indentation-strength method matched quite well. They revealed a good agreement with the temperature dependence of previously reported normalised fracture stresses. In addition to this, the effect of annealing on the mechanical properties of the material was also studied.

Keywords: Membranes; Fracture; Hardness; Strength; Toughness; Indentation

1. Introduction

Recently, the Oxyfuel technology with the rapid advancement in gas separation techniques has emerged as an important option for fossil fuelled power plants to ultimately capture CO_2.[1] Perovskite materials with ABO_3 structures (with rare earth metal ions in A-site and transition metal ions in B-site) appear to have a large potential for the application in such gas separation membranes.[1] The advantage of the perovskite membrane materials is their high oxygen separation capability. The fundamental mechanism responsible for the selective separation of oxygen from air is the diffusion of oxygen ions at elevated temperatures in the lattice of the perovskite material.[2–4] Although initially $SrCo_{1-y}Fe_yO_{3-d}$ was suggested as membrane material,[5–7] ordering of oxygen vacancies and associated reduction of the oxygen flux led to studies in which the partial replacement of Sr with Ba provided a higher level of oxygen non-stoichiometry and increased the permeability.[8,9]

Among the investigated perovskites, $Ba_{0.5}Sr_{0.5}Co_{0.8}Fe_{0.2}O_{3-d}$ (BSCF) appears to be one of the most promising oxygen permeable membrane materials.[6,9–11] Oxygen stoichiometry, oxygen permeation properties and the aspects of chemical stability of BSCF have been widely investigated.[6,7,12] By now also several reports are available on the thermal expansion behaviour and electrical conductivity of BSCF of different compositional variation.[13–15] Some recent works[16,17] have reported in great detail the charge density profile, atomic – isotropic displacement parameters and conductivity of BSCF based on data from synchrotron X-ray diffraction measurements, permitting an identification of the detailed temperature dependent oxygen transport mechanisms. Recently, Liu et al.[18] have studied the variation of crystal structure and chemical state of BSCF using XRD and X-ray photoelectron spectroscopy (XPS). In another recent work, Maier et al.[19] reported a significantly improved oxygen permeability in the case of BSCF thin layers.

Although the thermo-chemical aspects of BSCF have received a lot of attention, the information on the thermo-mechanical characteristics which are of crucial importance for design and engineering, is still limited to few publications, e.g. Huang et al.[20,21] In the studies of Huang et al., mainly a ring-on-

* Corresponding author. Tel.: +49 2461616964; fax: +49 2461616964.
E-mail address: j.malzbender@fz-juelich.de (J. Malzbender).

0955-2219/$ – see front matter © 2010 Elsevier Ltd. All rights reserved.
doi:10.1016/j.jeurceramsoc.2010.10.022

ring bending test configuration was used for measuring fracture stress and elastic modulus of BSCF as a function of temperature. In another paper Malzbender et al.[22] compared the elastic properties of BSCF materials obtained using different techniques. To the best of our knowledge, Huang et al.[20] reported for the first time the indentation fracture toughness of BSCF. However, the observed substantial discrepancy in the temperature-dependence of normalised fracture toughness and fracture stress remained unexplained. In an extension of this previous investigation, the aim of the present work was to explain this discrepancy and to do a systematic study on the micro-mechanical features of bulk BSCF material.

2. Experimental

The disc shaped BSCF samples were prepared at IEK-2, Forschungszentrum Jülich GmbH from powders supplied by Treibacher Industries AG, Austria. The powder was uniaxially pressed using a pressure of 105 MPa and sintered at 1000 °C for 12 h. Heating rate and cooling rate was 5 K/min. The density of the sample was measured with water emersion process (Archimedean method). The density of the sintered samples was 5.37 g/cm^3 with a porosity of 4.5%. Assuming a spherical geometry, the average dimension (diameter) of the equivalent grain size was 10 ± 4 μm. To study the effect of heat treatment, a batch of sintered pellets was annealed up to a temperature of 900 °C under partial pressure of oxygen, 10^{-5} mbar. It was assumed that the oxygen partial pressure is 1/5 of the measured total pressure. The absolute value of partial pressure was selected as per machine constraints. The heating and cooling rates were 3 K/min and 1 K/min, respectively. Subsequently after annealing, the samples were subjected to indentation tests from room temperature (RT) to 340 °C. The indentation characteristics of these annealed samples were compared with that of samples without annealing (mentioned as "as-received" samples). During indentation tests, the test temperature was too low (<350 °C) to cause oxygen mobility in the material and hence only 10 min' time was given for thermal equilibration of the oxygen content. Moreover the time was to be kept as low as possible to eliminate the scope of thermal drift. However, in case of mechanical measurements at higher temperature (>450 °C), sufficient time was provided at each temperature for equilibrating oxygen content. This time duration was optimised through number of test runs conducted at different temperatures.

The biaxial loadings in ring-on-ring bending tests were carried out for the disc specimens following the ASTM standard (C1499-05) using a universal testing machine (Instron 1362). Further details of this test along with the equations used for fracture stress and elastic modulus evaluation have been reported elsewhere.[20,22] Some discs were subjected to indentation on the tensile surface prior to bi-axial (ring-on-ring) fracture test to evaluate fracture toughness following the indentation-strength method reported by Chantikul et al.[23]

The discs, both with and without annealing, were ground and subsequently polished to mirror finish for the indentation tests with Vickers micro-indenter (H100, Fischer, Germany) and Vickers macro-test setups (Hardness Tester, Wolpert, Germany) at room temperature. The indentation load was varied from 10 mN to 10 N so as to see whether there was some indentation size effect for these perovskite materials. Micro-indentations with Vickers tip were also conducted at elevated temperatures using customer build CSM machine (CSM, Switzerland). Due to limitations of the CSM machine, tests could not be performed at a temperature > 340 °C. Interference between the indentation cracks and stress field around subsequent indentations was avoided by separating them to at least three times the indentation size. Loading and unloading curves were recorded from the micro-indentation studies using the in-built data acquisition software and the plasticity parameter (ratio of final depth to maximum depth) was evaluated. In addition to analysing hardness and elastic modulus on the basis of the standard procedure after Oliver and Pharr,[24] it has also been attempted to use the ratio of elastic and total indentation work to determine the elastic modulus.[25–27]

The indentations were observed using an optical microscope (CSM, Switzerland). In-built Image analysis software was applied to measure the length of the cracks as well as the indentation diagonals. These data were used subsequently to calculate the indentation hardness and fracture toughness. The subsurface damage zone under indentation and the profile of the indentation cracks were studied with a stereo-zoom and a scanning electron microscope (SEM, LEO1530, Zeiss, Germany). The relevant relationships for calculating the indentation fracture toughness were selected depending on the ratio of the crack length and indentation diagonal and also sub-surface crack profile. For each load, at least ten indentations were made to measure the diagonals and crack lengths.

3. Results and discussion

As shown in Fig. 1a the results of the hardness tests obtained with micro- (up to 1 N) and macro-indenter (>1 N) overlap well, however the hardness shows a strong load-dependence. Such indentation size effects (ISE) where the measured hardness depends on the deformed volume (load) have been widely reported for ceramics materials.[28] At low indentation loads (<0.1 N) the scatter in hardness values was ~25–30% and it decreased at higher loads (>1 N) to less than 10%.

The average room temperature hardness was 5.4 GPa (with indentation load of 1 N) and it decreased strongly with temperature (Fig. 1b), up to ~40% at around 340 °C similar to the percentage drop of elastic modulus of BSCF in bending tests.[20] Overall, the decrease of the hardness with temperature is comparable to that of conventional engineering ceramics like alumina, SiC, TiC.[28,29]

No signs of pile-up were observed around the indentation marks that might question the use of the relationship to determine the hardness. In most of the cases, the plasticity parameter was less than 0.7, the threshold above which pile-up around the indenter is supposed to occur.

The non-dissipated indentation energy ($W_{elastic}/W_{total}$) has been reported to be related to the elastic modulus,[25–27] which permits a convenient method to determine the elastic modulus

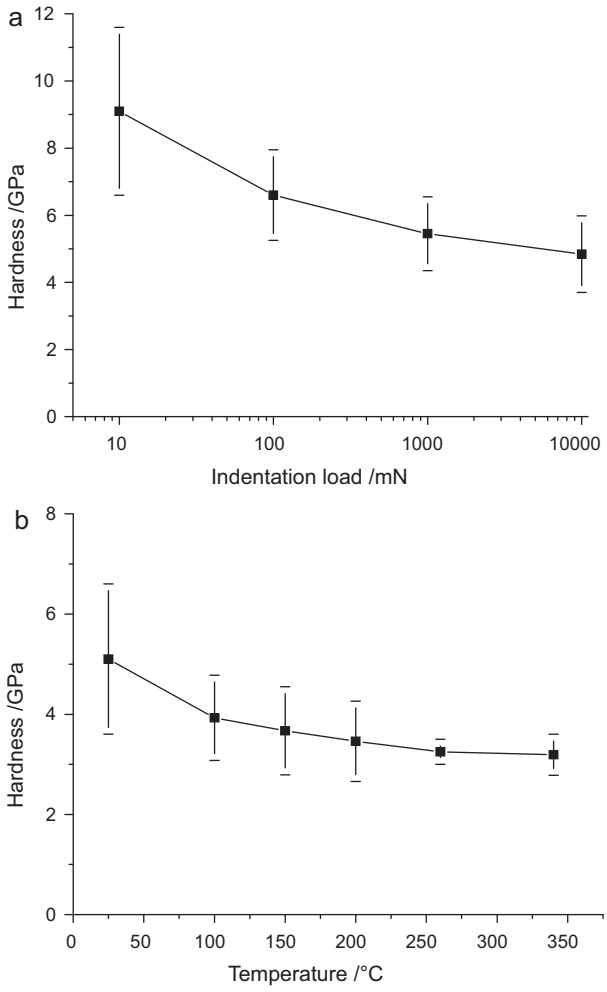

Fig. 1. Variation of hardness (a) with indentation load and (b) with temperature.

using:

$$E = 5.33H\left(\frac{W_{\text{total}}}{W_{\text{elastic}}}\right) \quad (1)$$

The advantage of this approach is that a drift effect at high temperatures that might occur during the unloading of the indenter does not have a strong impact on the energy ratio. It has been reported that the elastic modulus of BSCF obtained using bending test decreases due to a spin-transition of Co-ions and associated expansion by ~30% up to 200 °C.[20] The values obtained in the present study using Eq. (1) were consistently lower (around 10–15%) than those measured in bending test,[20] however a very similar decrease of ~25–30% was observed at a temperature of 200 °C in both tests (Table 1).

Table 1
Stiffness value (in GPa) calculated from the ratio of the dissipated energy for un-annealed (As received) BSCF.

Temperature/°C	*E*/GPa
RT	55 ± 4
200 °C	40 ± 3

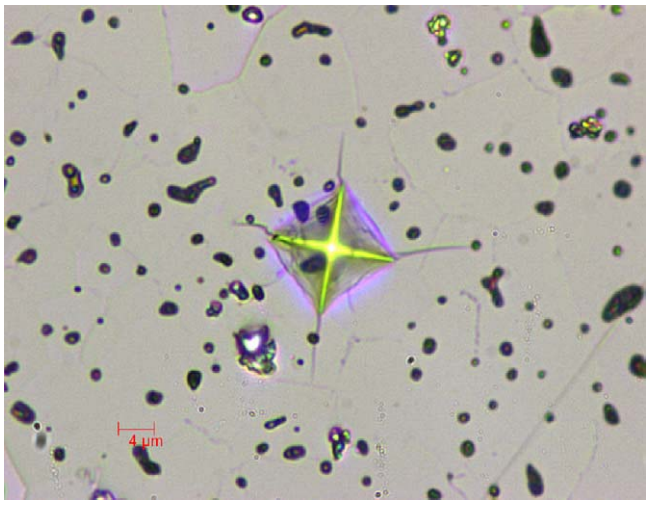

Fig. 2. A typical indentation imprint in BSCF at RT (load 0.6 N).

As typical for brittle ceramics, BSCF showed indentation cracks only above a threshold load. At loads higher than ~0.5 N cracks emerged clearly from the four corners of the impression (Fig. 2). Such indentation cracks have widely been used to estimate the fracture toughness of materials. In general the shape of indentation-cracks depends on the material composition, surface features, heat treatment and applied load. Different subsurface geometries like half-penny, radial-median and Palmqvist have been defined.[30–35] In the present work micrographs of the crack profiles were taken to define fracture path and crack geometry.

A careful observation revealed that the fracture path was transgranular independent of the crack length. The crack length at a particular load increased with increasing temperature (RT to 340 °C). A careful examination of the hardness data showed that although indentation cracks appeared at higher loads, they did not have any pronounced effect on the hardness values. In fact, from Fig. 1a, it was evident that substantial drop of hardness occurred well below the crack formation threshold of 0.6 N and there was only a small drop in hardness beyond that load.

For each indentation, the *c*/*a* ratio was calculated (with *c* being half crack length and *a* half diagonal) (Fig. 3). The ratio changed with indentation load. A simple statistical analysis revealed that at an indentation load of 1 N, 91% of the indentations (including all indentations at higher temperatures) had a $c/a < 3$ and 77%, a ratio of <2.5. At an indentation load of 0.6 N (the load typically used for indentations at elevated temperatures) more than 85% had a ratio of <2.5 and 73% a ratio of <2. So it can be summarized that in most of the cases the ratio was well below 2.5 or 3.

It should be noted that the use of indentation cracks to determine the fracture toughness is still under discussion in the literature, in particular regarding the existence of ideal radial-median crack profile at low values of *c*/*a*. In fact, the analysis method to be used for the indentation fracture toughness depends on crack shape, requiring the use of different relationships for the determination of the fracture toughness for different *c*/*a* regimes.[30–34] It has been suggested[31] that for Vickers indentation in the range of $c/a < 3$, the crack system is more likely of

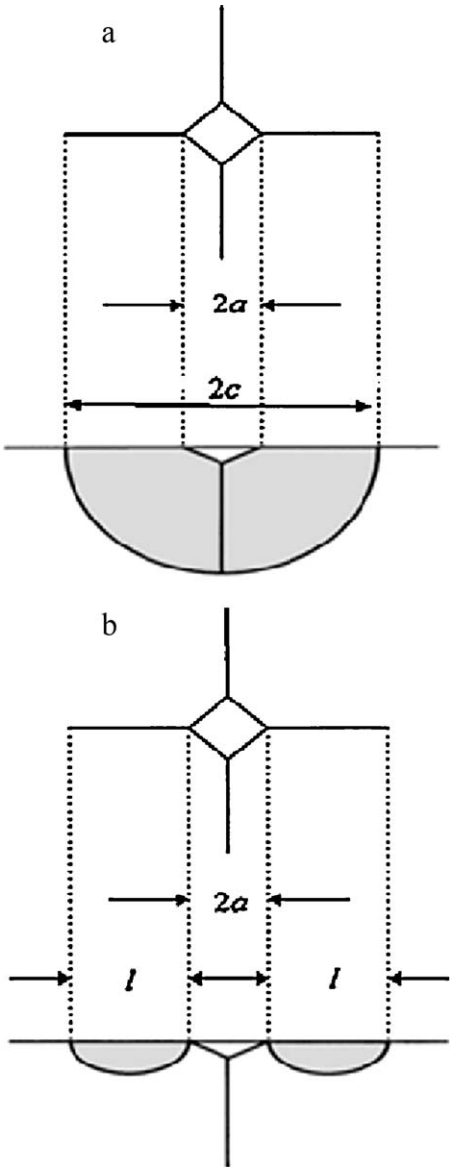

Fig. 3. Shematic drwing of (a) radial and (b) Palmqvist type crack profiles.

Palmqvist type and it changes to radial-median for larger c/a. In the present study, most of the indentation cracks showed $c/a > 3$ and it can be assumed to be Palmqvist in nature. Moreover, it was not possible to describe the data by a typical relationship for radial-median cracks (Fig. 4, $P \sim c^{1.5}$).[35] Therefore the analysis here was based on a relationship for Palmqvist type cracks for $l/a \approx 0.25$–2.5[31]:

$$K_{IC} = 0.0089\left(\frac{E}{H}\right)^{2/5}\left[\frac{P}{a\,l^{1/2}}\right] \quad (2)$$

In this relationship K_{IC} is the indentation fracture toughness, E the elastic modulus and P the load. It was found that the average value of indentation fracture toughness was 0.9 ± 0.1 MPa m$^{0.5}$ at room temperature. The value decreased significantly from RT to 200 °C, followed by a comparatively smaller drop at higher temperatures (Fig. 5). The uncertainty was ~10% at each temperature. From the toughness a critical crack length

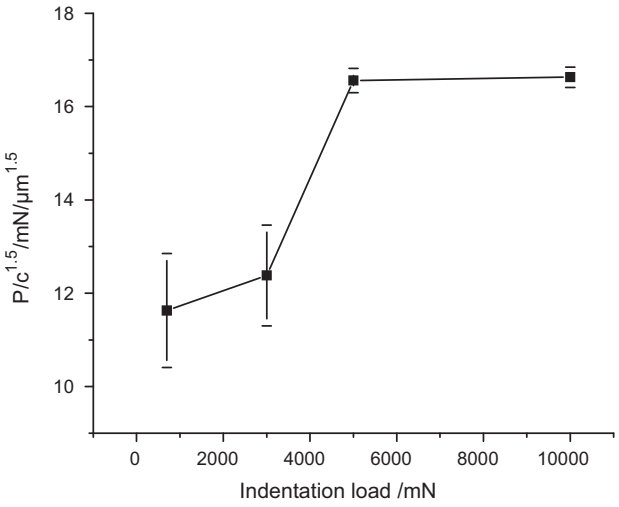

Fig. 4. Variation of the ratio $P/c^{1.5}$ with indentation load (P).

was determined using the geometry factor $Y = 1.25$ for standard semi-circular cracks[20] yielding a critical crack size of ~40 μm.

In a previous work, it had been reported that the normalised fracture toughness (ratio of fracture toughness at any temperature to that at RT) and fracture strength of BSCF[20] did not display identical temperature-dependence. However, a comparison of the temperature-dependence of newly derived indentation fracture toughness data with the previously reported strength values[20] in Fig. 5 revealed very good agreement.

The better agreement can be attributed to the fact that the indentation crack shape was better described by Palmqvist cracks contrary to the previous work where an ideal radial-median crack system was assumed. Furthermore the temperature-dependent variation of the factor E/H was also taken into account in the current work. It was based on the measured hardness and in addition the elastic moduli from ring-on-ring bending tests. It has been observed here that the ratio of E/H varied substantially with temperature, an observation which had not been considered in the previous investigation.[20]

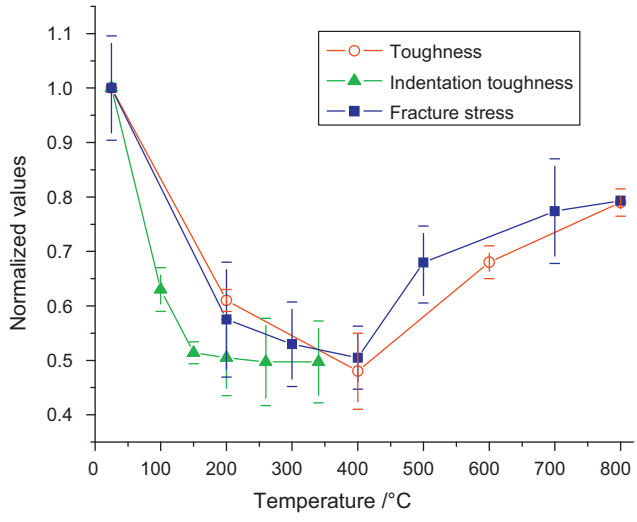

Fig. 5. Normalised indentation toughness, fracture stress and toughness (evaluated using the indentation-strength method).

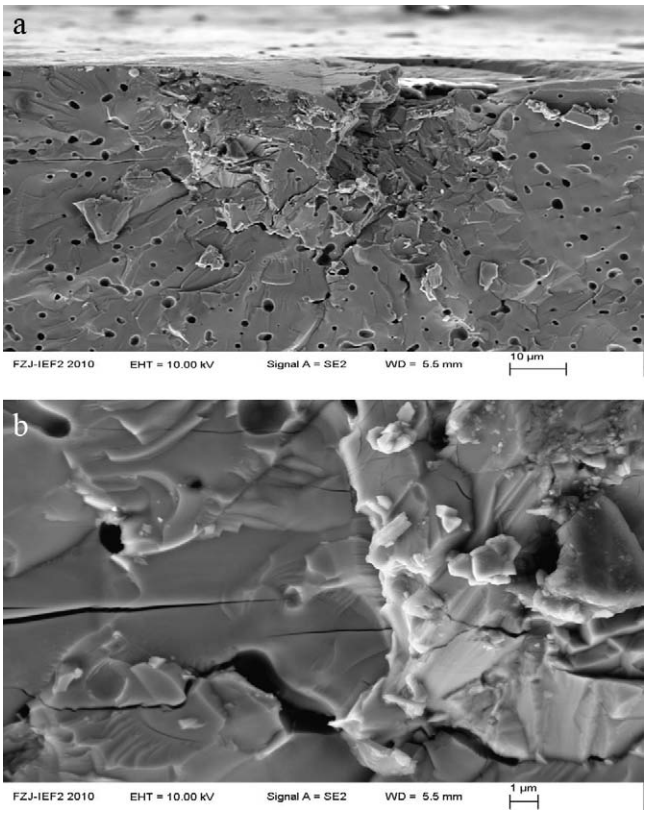

Fig. 6. Investigation of the crack profile. (a) SEM image of transgranular radial crack profile and damage below the indentation, (b) indications of damage accumulation and micro-cracking under the indentation.

Apart from the indentation load of 0.6 N (generally used in the present study at different temperatures including RT), the indentation fracture toughness was also evaluated at higher loads ranging from 5 N to 50 N ($c/a \sim 3$). But at indentation loads >20 N, severe lateral chipping occurred in most cases. To investigate the subsurface crack profile, a series of indentations were made with a load ≥5 N on polished samples along a pre-defined straight line. Then the samples were broken carefully along this line. The cross-sections were investigated with stereo-zoom microscope. A typical sub-surface profile of an impression after loading to 10 N is shown in Fig. 6a. The microstructure of the sub-surface indentation crack profile reveals that the crack path was fully transgranular and there was severe damage associated with micro-cracking (Fig. 6b). It may be noted in Fig. 6a that the area just beneath the indentation had a comparatively lower number of pores than the surrounding sub-surface region. It shows that due to plastic deformation the pores collapsed in that area. Based on the statistical data for c/a (consistently greater than 3) and the microscopic evidence, the indentation toughness was determined for this high load indentations using the classical relationship for median radial cracks[35]:

$$K_{IC} = 0.016\left(\frac{E}{H}\right)^{1/2}\left[\frac{P}{c^{3/2}}\right] \quad (3)$$

Table 2 summarises the room temperature indentation fracture toughness values for the low and high load range as obtained using the respective relationships for Palmqvist and median-radial cracks. It can be seen that the toughness values were larger at higher loads. With higher indentation loads, there was decrease in hardness due to indentation size effect whereas the elastic modulus was almost independent of load. So the ratio of hardness to elastic modulus increased. The higher value of toughness at higher load can be attributed to this behaviour. The overall average indentation fracture toughness is 1.2 ± 0.3 MPa m$^{0.5}$.

Table 2
Room temperature (RT) indentation fracture toughness of dense BSCF.

Load/kg	K_{IC} in MPa m$^{0.5}$
0.06	0.9 ± 0.2
0.5	1.2 ± 0.1
1	1.3 ± 0.1
2	1.4 ± 0.1
5	1.44 ± 0.15

Although it was proposed by Anstis et al.[35] that the indentation fracture toughness can be determined with an accuracy of more than 30–40%, in the present study, the BSCF material was also analysed in addition using the so-called indentation-strength method.[23] The indentation strength method is based on the fracture of pre-indented specimens in a bi-axial, ring-on-ring bending test configuration. Following the guidelines given by Chantikul et al.[23], the method requires that indentation cracks should be radial-median, large enough to act as fracture initiation defects and the maximum crack depth should be <1/10 of the specimen thickness. Pre-tests revealed that a load of 20 N leads to cracks which satisfied these boundary conditions.

The average pre-test indentation crack length c was measured to be 90–120 μm (specimen thickness 800–1000 μm). The pre-indentation is supposed to induce flaws that are larger than the native flaws of the material which can be checked conveniently by the subsequent reduction in fracture stress. The variation of the fracture stress in bending test with pre-indentation load in Fig. 7 confirmed that with indentation loads of ≥20 N indentation cracks initiated the fracture. In fact, the product of fracture

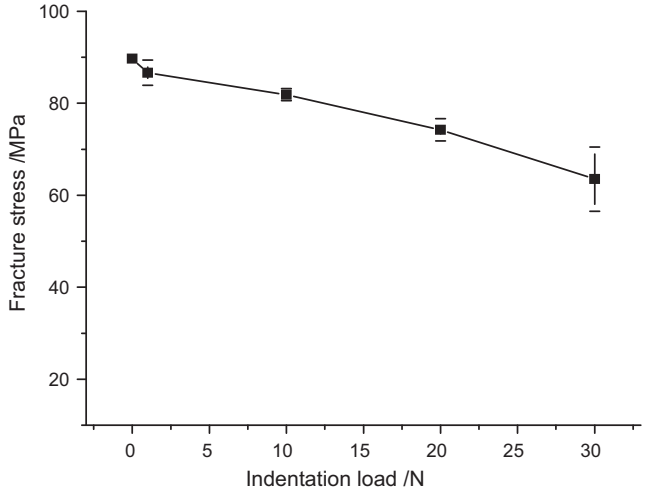

Fig. 7. Variation of fracture stress with indentation load for pre-indented samples.

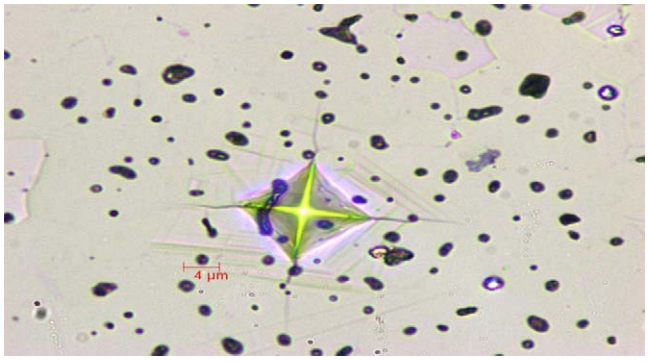

Fig. 8. Shear-deformation bands surrounding indentation at 86 °C for annealed BSCF.

stress σ_f and the indentation load $P^{1/3}$ was constant which is the basic verification of the indentation strength method,[23] since:

$$K_{IC} = 0.59\left(\frac{E}{H}\right)^{1/8}[\sigma_f P^{1/3}]^{3/4} \quad (4)$$

Using this relationship, an average value of room temperature fracture toughness of 1.24 MPa $m^{0.5}$ (uncertainty 5%) could be determined for the pre-indented BSCF specimens. It has been suggested that the critical crack length is larger than the initial length of the radial crack formed during indentation. Although it has been suggested that this should lead to an error of ~27%[35] the value was in good agreement with the indentation fracture toughness measured using the standard indentation technique.

Indentation-strength tests at elevated temperatures (200 °C, 400 °C, 600 °C and 800 °C respectively) were carried out using the same principle. The thermal annealing followed the procedure outlined in earlier reports[20,21] where the equilibration times at different temperatures were optimised through repeated tests. The temperature-dependence of the obtained fracture toughness was in good agreement with that of the indentation fracture toughness and conventional bending fracture stress (Fig. 5). The fracture toughness decreased by almost 50% up to 400 °C, while at 800 °C it recovered to 70% of the RT value, similar to

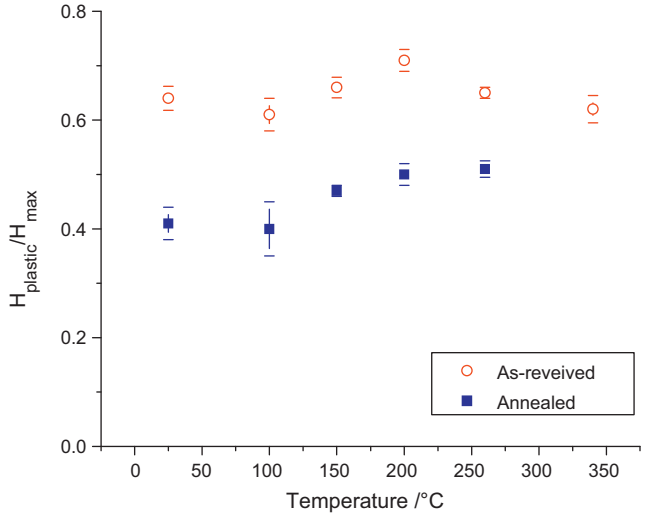

Fig. 9. Variation of plasticity parameter with temperature.

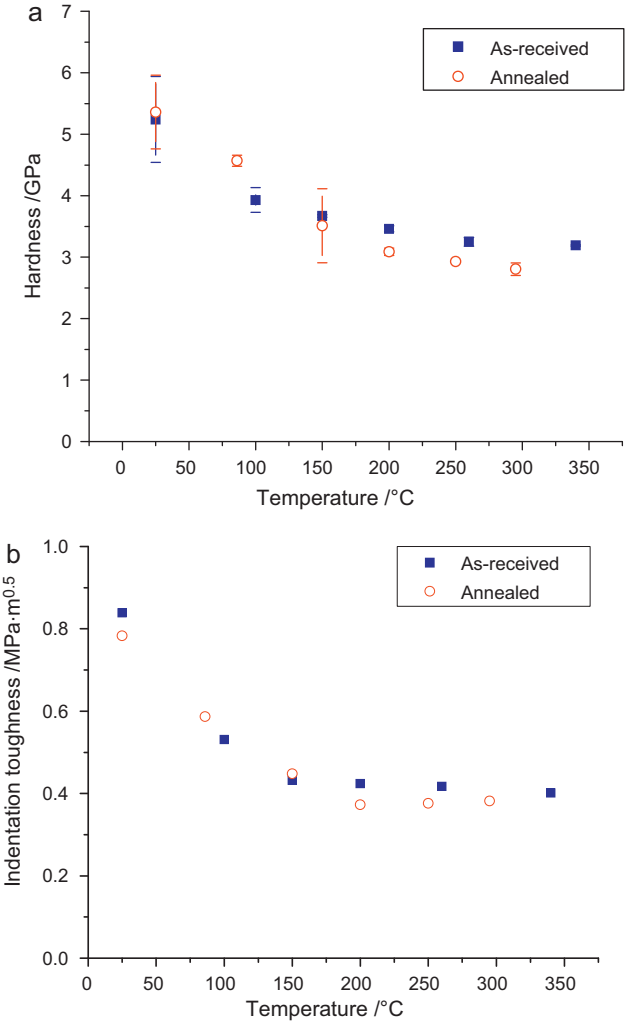

Fig. 10. Temperature dependence of (a) hardness and (b) fracture toughness.

temperature-dependent variation of the average fracture stress reported in.[20]

For vacuum annealed (10^{-5} mbar) specimens, the shear-deformation bands (Fig. 8) were visible at a significantly lower temperature, 86 °C compared to 260 °C in samples without annealing ("As-received"). This suggests that vacuum annealing of BSCF lead to an easier mode of shear deformation. However, the ratio of maximum depth to final depth (i.e. plasticity parameter), did not support it. In fact, contrary to the expectation, this ratio was generally larger for un-annealed ("As-received") samples than for the annealed ones (Fig. 9). This might have been due to the fact that the annealed samples showed more total deformation as well as more elastic recovery than samples without annealing. Overall, the differences in the temperature dependence of hardness and toughness (Fig. 10a and b) were within the limits of uncertainty, although the hardness for the annealed specimens appeared to decrease stronger.

From the results given above it appears that fracture toughness, hardness and elastic modulus had similar temperature dependence up to a temperature ~200 °C. Hardness is a combined parameter depending on elastic, yield strength, indenter angle but also crack formation and crack growth. No recovery

Table 3
Stiffness value (in GPa) calculated from the ratio of the dissipated energy for annealed BSCF.

Temperature/°C	*E*/Gpa
RT	48 ± 3
250 °C	32 ± 4

effect was found for hardness at higher temperatures contrary to the elastic modulus. Fracture toughness and elastic modulus revealed similar decreases till ∼200 °C (Table 3). Above ∼250 °C the elastic modulus increased which might lead to associated changes in fracture toughness, since fracture toughness is a parameter that depends on elastic modulus and fracture energy of a material.

4. Conclusion

It may be concluded from the present work that both indentation crack measurement and pre-indentation technique (indentation-strength technique) resulted in a very similar temperature-dependence of the fracture toughness. The toughness values obtained from indentation strength method were compared with the values calculated from indentation cracks not only at room temperature but also at higher temperatures. Apart from similar absolute values at room temperature, even at elevated temperatures, approximately the same percentage drop of toughness was noticed in both the methods. The pre-indentation technique permitted results to be obtained over a wider temperature range with a low uncertainty (∼20%).

Indentation toughness evaluation at high temperature is often considered to be difficult, due to limitations of available testing devices. The indentation-strength method can be a useful alternative especially for membrane materials that will be used at high temperatures in technical application. In this method, there are no special requirements on the sample preparation which eases the determination methodology. Particularly for porous membrane materials where indentation crack-measurement is difficult, this method is expected to be an effective tool for toughness evaluation. A measurement of the fracture toughness using the indentation-strength method of specimens that have been exposed to the normal laboratory environment for 6 months did not show any decrease in toughness, indicating that slow crack growth is not of major relevance for this perovskite material at room temperature.

The normalised values of fracture stress and fracture toughness revealed good agreement. It appears that the strong decrease in fracture toughness was coupled to the decrease in elastic modulus and both are related to the inherent bond strength. In two recent studies[16,17] it has been shown that within the temperature range 300–500 K substantial variation in the charge density profile of different A–O and B–O bonds occurred for BSCF and there was a decrease in bond-strength of certain covalent bonds. Since there is no indication of phase change in this temperature range, changes in bond strength due to a distortion of the BO_6 octahedron can be the reason for such simultaneous decrease in elastic modulus and fracture toughness. In fact, with ABO_3 perovskite structures like BSCF having Jahn Teller ion like Co at its B-site, a spin transition of Co-ion with temperature, a distortion of the crystal structure and a change in bond strength can contribute in a complex manner to result in such anomalous mechanical behaviour. However, still further in-depth studies are needed for quantitative as well as qualitative estimation of the structural distortion with temperature.

Acknowledgements

Financial support from the Helmholtz Association of German Research Centres (Initiative and Networking Fund) through the Helmholtz Alliance MEM-BRAIN is gratefully acknowledged. The authors would like to express their gratitude to M. Lipinska-Chwalek for the discussions on the use of the indentation-strength method and R. Küppers for the very good experimental and technical support. Special thanks go to Dr. W. Meulenberg and Dr. S. Bauman who provided the BSCF specimens for the present work.

References

1. Cheng JH, Navrotsky A, Zhou XD, Anderson HU. Thermochemistry of $La_{1-x}Sr_xFeO_{3-delta}$ solid solutions ($0.0 \le x \le 1.0, 0.0 \le$ delta ≤ 0.5). *Chem Mater* 2005;**17**(April 19 (8)):2197–207.
2. Gellings PJ, Bouwmeester HJM. *Handbook of solid state electrochemistry*. New York: CRC-Press; 1997. p. 656.
3. Liu LM, Lee TH, Qiu L, Yang YL, Jacobson AJ. A thermogravimetric study of the phase diagram of strontium cobalt iron oxide, $SrCo_{0.8}Fe_{0.2}O_{3-delta}$. *Mater Res Bull* Jan 1996;**31**(1):29–35.
4. Teraoka Y, Zhang HM, Okamoto K, Yamazoe N. Mixed ionic-electronic conductivity of La_{1-X}srxco$_{1-Y}$feyo$_{3-Delta}$ perovskite-type oxides. *Mater Res Bull* 1988;**23**(January (1)):51–8.
5. Kruidhof H, Bouwmeester HJM, Vondoorn RHE, Burggraaf AJ. Influence of order–disorder transitions on oxygen permeability through selected nonstoichiometric perovskite-type oxides. *Solid State Ionics* 1993;**63**(September (5)):816–22.
6. McIntosh S, Vente JF, Haije WG, Blank DHA, Bouwmeester HJM. Structure and oxygen stoichiometry of $SrCo_{0.8}Fe_{0.2}O_{3-elta}$ and $Ba_{0.5}Sr_{0.5}Co_{0.8}Fe_{0.2}O_{3-delta}$. *Solid State Ionics* 2006;**177**(October 15 (19–25)):1737–42.
7. Svarcova S, Wiik K, Tolchard J, Bouwmeester HJM, Grande T. Structural instability of cubic perovskite $Ba_xSr_xSr_{1-x}Co_{1-y}FeyO_{3-delta}$. *Solid State Ionics* 2008;**178**(February 15 (35–36)):1787–91.
8. Shao ZP, Xiong GX, Tong JH, Dong H, Yang WS. Ba effect in doped $Sr(Co_{0.8}Fe_{0.2})O_{3-delta}$ on the phase structure and oxygen permeation properties of the dense ceramic membranes. *Sep Purif Technol* Oct 1 2001;**25**(1–3):419–29.
9. Sunarso J, Baumann S, Serra JM, et al. Mixed ionic-electronic conducting (MIEC) ceramic-based membranes for oxygen separation. *J Membr Sci* Jul 15 2008;**320**(1–2):13–41.
10. Vente JF, Haije WG, Rak ZS. Performance of functional perovskite membranes for oxygen production. *J Membr Sci* 2006;**276**(May 1 (1–2)):178–84.
11. Shao ZP, Yang WS, Cong Y, Dong H, Tong JH, Xiong GX. Investigation of the permeation behavior and stability of a $Ba_{0.5}Sr_{0.5}Co_{0.8}Fe_{0.2}O_{3-delta}$ oxygen membrane. *J Membr Sci* Jul 1 2000;**172**(1–2):177–88.
12. Ovenstone J, Jung JI, White JS, Edwards DD, Misture ST. Phase stability of BSCF in low oxygen partial pressures. *J Solid State Chem* 2008;**181**(March (3)):576–86.
13. Wei B, Lu Z, Huang XQ, Miao J, Sha X, Xin X, et al. Crystal structure, thermal expansion and electrical conductivity of perovskite oxides $Ba_xSr_{1-x}Co_{0.8}Fe_{0.2}O_{3-delta}$ ($0.3 \le x \le 0.7$). *J Eur Ceram Soc* Sep 2006;**26**(13):2827–32.

14. Li DC, Liu W, Zhang HL, Jiang GS, Chen CS. Fabrication, microstructure, mechanical strength and oxygen permeation of Ba(Sr)Zr(CoFe)O-3-particles-dispersed $Ba_{0.5}Sr_{0.5}Co_{0.8}Fe_{0.2}O_{3-delta}$ mixed-conducting composites. *Mater Lett* 2004;**58**(April (10)):1561–4.
15. van Veen AC, Rebeilleau M, Farrusseng D, Mirodatos C. Studies on the performance stability of mixed conducting BSCFO membranes in medium temperature oxygen permeation. *Chem Commun* 2003;(1):32–3.
16. Itoh T, Shirasaki S, Fujie Y, Kitamura N, Idemoto Y, Osaka K, et al. Study of charge density and crystal structure of $(La_{0.75}Sr_{0.25})MnO_{3.00}$ and $(Ba_{0.5}Sr_{0.5})(Co_{0.8}Fe_{0.2})O_{2.33-delta}$ at 500–900 K by in situ synchrotron X-ray diffraction. *J Alloys Compds* Feb 18 2010;**491**(1–2):527–35.
17. Itoh T, Nishida Y, Tomita A, Fujie Y, Kitamura N, Idemoto Y, et al. Determination of the crystal structure and charge density of $(Ba_{0.5}Sr_{0.5})(Co_{0.8}Fe_{0.2})$O-2.33 by Rietveld refinement and maximum entropy method analysis. *Solid State Commun* 2009;**149**(January (1–2)):41–4.
18. Liu BW, Zhang Y, Tang LD. X-ray photoelectron spectroscopic studies of $Ba_{0.5}Sr_{0.5}Co_{0.8}Fe_{0.2}O_{3-delta}$ cathode for solid oxide fuel cells. *Int J Hydrogen Energy* 2009;**34**(January (1)):435–9.
19. Wang L, Merkle R, Maier J, Acarturk T, Starke U. Oxygen tracer diffusion in dense $Ba_{0.5}Sr_{0.5}Co_{0.8}Fe_{0.2}O_{3-delta}$ films. *Appl Phys Lett* 2009;**94**(February 16 (7)).
20. Huang BX, Malzbender J, Steinbrech RW, Grychtol P, Schneider CM, Singheiser L. Anomalies in the thermomechanical behavior of $Ba_{0.5}Sr_{0.5}Co_{0.8}Fe_{0.2}O_{3-delta}$ ceramic oxygen conductive membranes at intermediate temperatures. *Appl Phys Lett* 2009;**95**(August 3 (5)): 051901.
21. Huang BX, Malzbender J, Steinbrech RW, Singheiser L. Mechanical properties of $La_{0.58}Sr_{0.4}Co_{0.2}Fe_{0.8}O_{3-delta}$ membranes. *Solid State Ionics* 2009;**180**(March 9 (2–3)):241–5.
22. Malzbender J, Huang B, Mönch J, Steinbrech RW. A comparison of results obtained using different methods to assess the elastic properties of ceramic materials exemplified for $Ba_{0.5}Sr_{0.5}Co_{0.8}Fe_{0.2}O_{3-\delta}$. *J Mater Sci* 2010;**45**(5):1227–30.
23. Chantikul P, Anstis GR, Lawn BR, Marshall DB. a critical-evaluation of indentation techniques for measuring fracture-toughness. 2. Strength method. *J Am Ceram Soc* 1981;**64**(9):539–43.
24. Oliver WC, Pharr GM. An improved technique for determining hardness and elastic-modulus using load and displacement sensing indentation experiments. *J Mater Res* 1992;**7**(June (6)):1564–83.
25. Malzbender J, de With G. Indentation load-displacement curve, plastic deformation, and energy. *J Mater Res* 2002;**17**(February (2)):502–11.
26. Cheng YT, Cheng C-M, Li Z. Fundamentals of nanoindentation and nanotribology II. In: Baker SPJRFC, Corcoran SG, Moody NR, editors. *MRS proceedings*, vol. 649. 2000.
27. Venkatesh TA, Van Vliet KJ, Giannakopoulos AE, Suresh S. Determination of elasto-plastic properties by instrumented sharp indentation: guidelines for property extraction. *Scr Mater* 2000;**42**(April 21 (9)):833–9.
28. Lankford J. Comparative-study of the temperature-dependence of hardness and compressive strength in ceramics. *J Mater Sci* 1983;**18**(6):1666–74.
29. Loladze TN, Bokughava GV, Davidova GE. In: Westbrook JH, Conrad H, editors. *The science of hardness testing and its research applications*. Ohio: American Society for Metals in Metals Park; 1973. p. 520.
30. Ponton CB, Rawlings RD. Vickers indentation fracture toughness test. Part 1. Review of literature and formulation of standardised indentation toughness equations. *Mater Sci Technol* 1989;**5**(9):865–72.
31. Niihara K, Morena R, Hasselman DPH. Evaluation ofKIc of brittle solids by the indentation method with low crack-to-indent ratios. *J Mater Sci Lett* 1981;**1**(1):13–6.
32. Evans AG, Charles EA. Fracture toughness determinations by indentation. *J Am Ceram Soc* 1976;**59**(7–8):371–2.
33. Evans AG, Wilshaw TR. Quasi-static solid particle damage in brittle solids. 1. Observations, analysis and implications. *Acta Metall* 1976;**24**(10):939–56.
34. Dawihl W. *Z Metallkd* 1964;**55**(2):231.
35. Anstis GR, Chantikul P, Lawn BR, Marshall DB. A critical-evaluation of indentation techniques for measuring fracture-toughness. 1. Direct crack measurements. *J Am Ceram Soc* 1981;**64**(9):533–8.